# Supporting Information

# Flow Battery Electroanalysis 2: Influence of Surface Pretreatment on Fe(III/II) Redox Chemistry at Carbon Electrodes

Tejal V. Sawant and James R. McKone*

*Department of Chemical and Petroleum Engineering, Swanson School of Engineering, University of Pittsburgh, Pittsburgh, PA 15261, USA*

E-mail: jmckone@pitt.edu

## Tabulated $Fe^{3+/2+}$ kinetics

Table S1 presents reported kinetics data for $Fe^{3+/2+}$ redox chemistry at carbon electrodes. The rate constants, all of which were collected using RDE voltammetry, varied over nearly three orders of magnitude. Reported $\alpha$ values are close to 0.5 in most cases, while some reports did not explicitly include $\alpha$ values.

Table S1: Kinetics of $Fe^{3+/2+}$ as reported in literature

| **Electrode** | **Rate constant $k^0$ (cm/s)** | $\alpha$ | **Measuring technique** | **Supporting electrolyte** | **[Fe]** | **Ref.** |
|---|---|---|---|---|---|---|
| GC | 4.4 x $10^{-3}$ | 0.5 | RDE | 0.1 M HCl | | [1] |
| GC | 1 x $10^{-3}$ | 0.5 | RDE | 0.3 M HCl | | [1] |
| GC | 2.9 x $10^{-3}$ | 0.5 | RDE | 0.1 M $HNO_3$ | | [1] |
| GC | $>10^{-2}$ | 0.57 | RDE | 0.1-1 M $HClO_4$ | | [1] |
| GC | 1.3 x $10^{-3}$ | 0.5 | RDE | 0.1 M $H_2SO_4$ | | [1] |
| Carbon paste | 5.4 x $10^{-5}$ | 0.63 | RDE | 1 M $H_2SO_4$ | | [2] |
| Carbon paste | 8.5 x $10^{-5}$ | | RDE | 0.1 M HCl | | [2] |
| GC | 2.3 x $10^{-3}$ | | RDE | 0.2 M $HClO_4$ | 5 mM | [3] |
| GC | 2.3 x $10^{-4}$ | | RDE | 1 M NaCl | 0.1 M | [4] |
| Pyrolytic graphite | 5.2 x $10^{-4}$ | | RDE | 4 M HCl | 0.1 M | [5] |

## Peak current vs. scan rate

We performed cyclic voltammetry over a series of scan rates from 10 to 200 mV/s (Figure S1). Figure S2 plots the resulting peak current versus square root of scan rate, which show linear behavior as expected from a diffusional process.

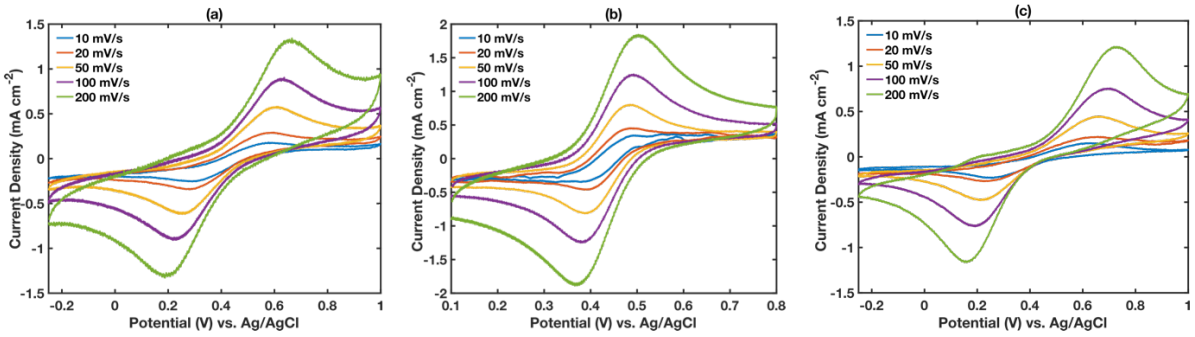


Figure S1: Cyclic voltammograms of (a) AC/IPA treated GC, (b) electrochemically treated GC and (c) $H_2O_2$ treated GC electrodes depicting scan rate dependence in an electrolyte containing 5mM $FeCl_2$ and 5mM $FeCl_3$ in 0.5 M HCl(aq).

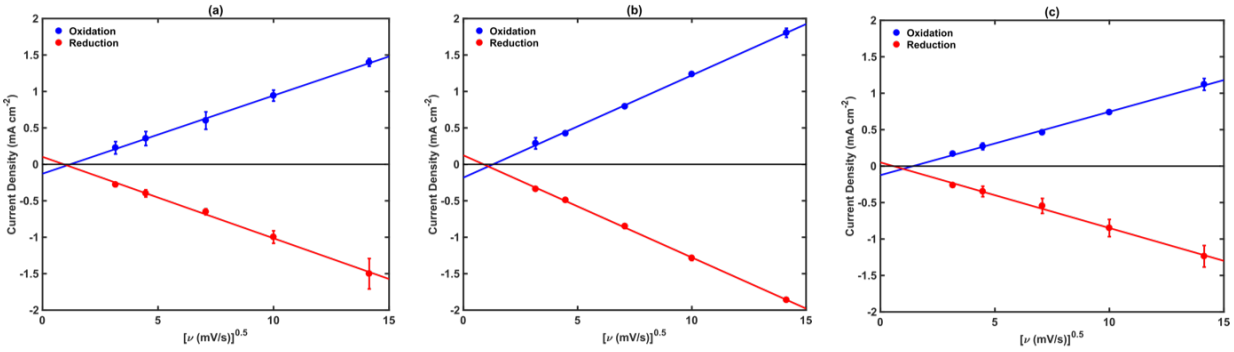


Figure S2: Peak current density vs. square root of scan rate for (a) AC/IPA treated GC, (b) electrochemically treated GC and (c) $H_2O_2$ treated GC electrodes in an electrolyte containing 5mM $FeCl_2$ and 5mM $FeCl_3$in 0.5 M HCl(aq). Error bars represent standard devation from the mean of 3 replicates.

## Kinetics estimates from CV data

To estimate electron-transfer kinetics directly from CV data, we followed the method reported by Nicholson, who showed that the relationship between $\Delta E_p$ and scan rate can be used to determine $k_0$.[6] We first extracted the following mathematical relationship between $\Delta E_p$ and an empirical parameter $\psi$ from Nicholson's report:

$$\Delta E_p \cdot n = 0.054 + 0.03103\psi^{-0.7078} \tag{1}$$

Nicholson showed that $\psi$ can be related to the apparent electron-transfer rate constant $k_{0,app}$ via the following equation:

$$\psi = \nu^{-\frac{1}{2}} k_{0,app} \left[\frac{\pi n F D}{RT}\right]^{-\frac{1}{2}} \tag{2}$$

such that a plot of $\psi$ vs $\nu^{-0.5}$ should give a line with y intercept that is near zero and a slope that is proportional to $k_0$. Figure S3 shows the corresponding plots for $Fe^{3+/2+}$ voltammetric data at carbon electrodes prepared by the three different methods over an extended range of scan rates from 10–3000 mV/s.

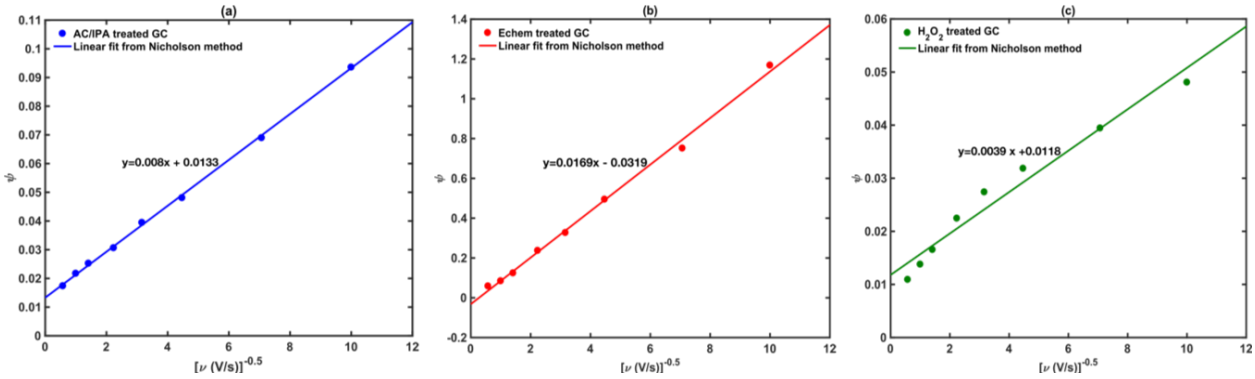


Figure S3: Plots of $\psi$ versus inverse square root of scan rate along with least-squares fits over a range of scan rates from 10–3000 mV/s for (a) AC/IPA treated GC, (b) electrochemically treated GC and (c) $H_2O_2$ treated GC

The data for AC/IPA and electrochemically treated carbon both gave excellent linear fits, whereas the $H_2O_2$ treated carbon gave a considerably poorer fit, which is consistent with the greater relative uncertainty we found in the RDE results for these surfaces. Table S2 collects apparent $k_0$ values ($k_{0,app}$) extracted from the slopes of these data along with the corresponding $j_0$ values calculated for a 5 mM reactant concentration under the assumption that the diffusivity was 4 x $10^{-6}$ $cm^2/s$ and the relationship between $k_{0,app}$ and $j_0$ obeys the following equation:

$$j_0 = nFCk_{0,app} \tag{3}$$

These $j_0$ values agree reasonably well with those reported from RDE results in the main text. However, because these results relied on a mathematical fit to Nicholson's empirical relation, we recommend that they be treated only as an order-of-magnitude estimate of reaction kinetics. Thus, we reported only the relative electron transfer rates in the main text.

Table S2: $j_0$ and $k_{0,app}$ obtained from analysis of voltammetry data

| Electrode | $k_{0,app}$ (cm/s) | $j_0$ (mA/cm$^2$) |
|---|---|---|
| AC/IPA treated GC | 2.4 x $10^{-4}$ | 0.12 |
| Electrochemically treated GC | 3.7 x $10^{-3}$ | 1.8 |
| $H_2O_2$ treated GC | 1.2 x $10^{-4}$ | 0.06 |

## Results of conventional Butler-Volmer fits with constrained $\alpha$ values

Figure S4 reports conventional Butler-Volmer fits of kinetics data obtained by constraining the fit to $\alpha_{ox} + \alpha_{red} = 1$. These results show a clear deviation in the fits for all 3 electrode surface treatments, which were resolved by allowing the symmetry factors to vary arbitrarily between 0 and 1 as shown in the main text. Such a deviation is consistent with a reaction mechanism involving both electrochemical and chemical elementary steps.

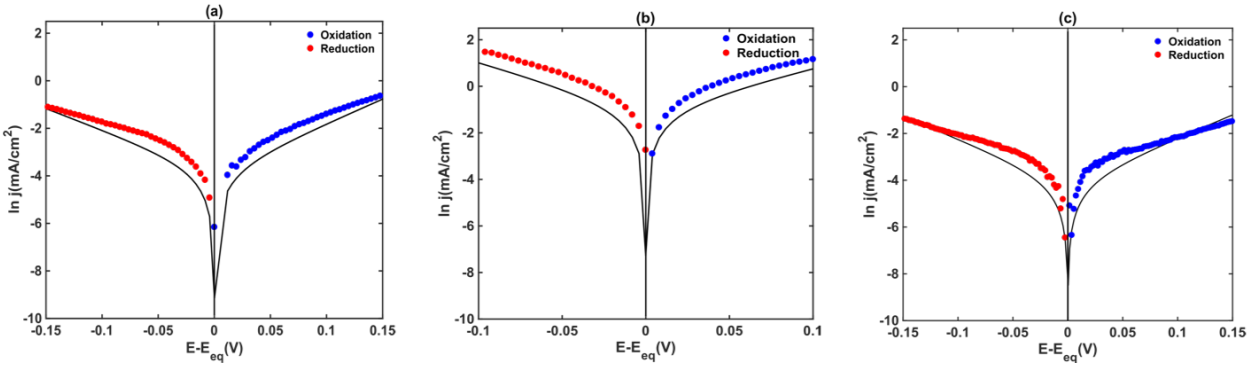


Figure S4: Transport free polarization data for (a) AC/IPA treated GC, (b) electrochemically treated GC and (c) $H_2O_2$ treated GC electrodes in electrolyte containing 5mM $FeCl_2$ and 5mM $FeCl_3$ in 0.5 M HCl(aq). The black lines correspond to fits using the Butler-Volmer equation where the symmetry factors were constrained to $\alpha_{ox} + \alpha_{red} = 1$.

## Surface roughness effects

One potential explanation for the differences that we observed in $Fe^{3+/2+}$ electron transfer kinetics is simply that the electrochemical surface treatment significantly influences electode surface area, resulting in differences in the geometric exchange current density. Thus, we made additional efforts to characterize surface areas using SEM, AFM, and interfacial capacitance measurements.

Figures S5 and S6 show SEM and AFM images of GC electrodes after each treatment. These data clearly show that we were unable to eliminate polishing damage in the form of sub-micron scratches. However, qualitative comparisons of these images showed mutually similar morphologies, and RMS roughness values extracted from AFM data for all three electrodes were

nearly identical at ∼5 nm. Although we cannot rule differences in roughness on a very small length scale (e.g., a few nm or less) that would not be readily apparent from SEM or AFM, we expect that these differences would also manifest as differences in the density of crystallographic defects, which was not apparent from Raman measurements. Thus, we conclude that the electrochemical and $H_2O_2$ treatments resulted in minimal increases in electrode surface area.

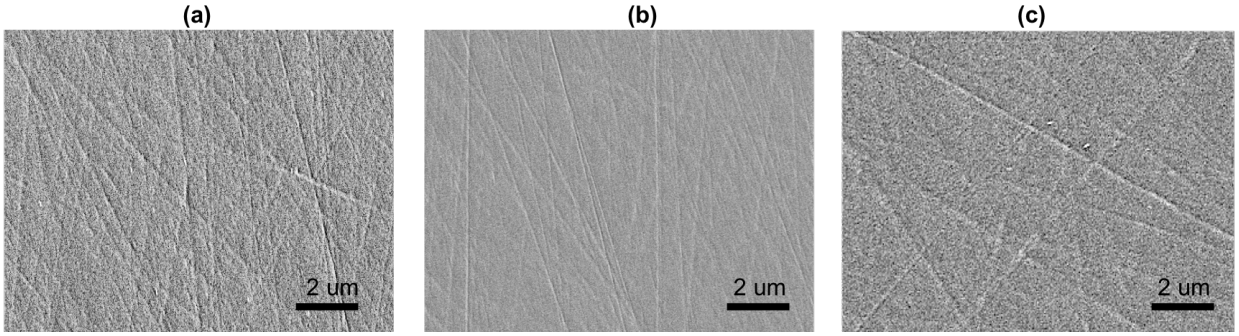


Figure S5: Scanning electron micrographs of (a) AC/IPA treated GC, (b) electrochemically treated GC and (c) $H_2O_2$ treated GC

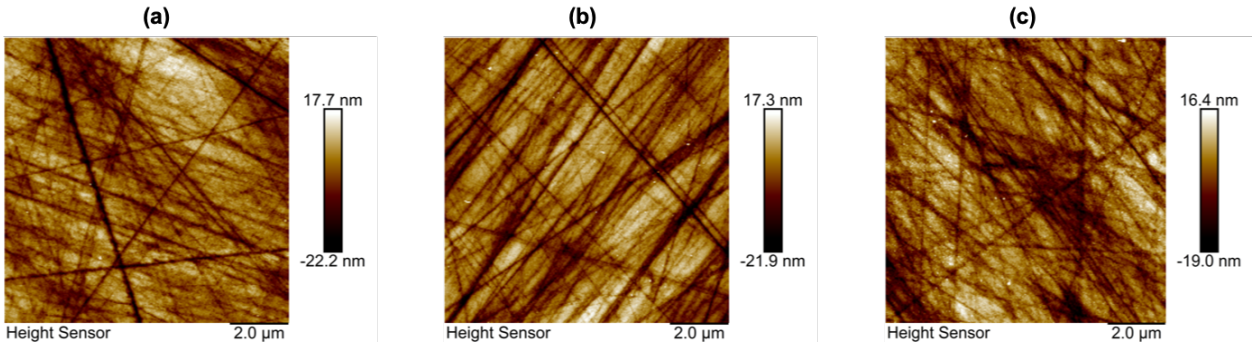


Figure S6: Atomic force micrographs of (a) AC/IPA treated GC, (b) electrochemically treated GC and (c) $H_2O_2$ treated GC

Figure S7 overlays representative CV data for stationary GC electrodes in 0.5 M $H_2SO_4$ solution over the potential range from -0.2 to 0.6 V vs. Ag/AgCl after each surface treatment. In the absence of a redox couple, the data in this range are representative of the interfacial capacitance of the electrodes resulting from the combination of double-layer charging and pseudocapacitance from redox-active surface groups. Whereas prior work involving similar solvent treatments resulted in interfacial capacitance values on the order of 50–100 $\mu$F/cm$^2$,[7] we found AC/IPA treated

electrodes gave values on the order of 500 $\mu$F/cm$^2$. Thus, these results are consistent with the residual roughness we observed by SEM and AFM and imply a roughness factor (defined as the quotient of electrochemically active area and geometric area) of 5–10. Interestingly, the interfacial capacitance increased very slightly (from 485 to 525 $\mu$F/cm$^2$) after the electrochemical surface treatment, whereas it decreased considerably to $\sim$200 $\mu$F/cm$^2$ after the $H_2O_2$ treatment. This contrasted with our expectation that the capacitance would increase slightly in both cases due to the generation of additional redox-active surface groups. However, the XPS data in the main text show that the distribution of surface functionalities between the electrochemical and $H_2O_2$ treatments varied considerably; we therefore speculate that the $H_2O_2$ treatment predominantly resulted in "redox silent" surface species. In any case, these data are not consistent with an explanation where capacitance is proportional to surface area and increased surface area alone drives increased reaction rates.

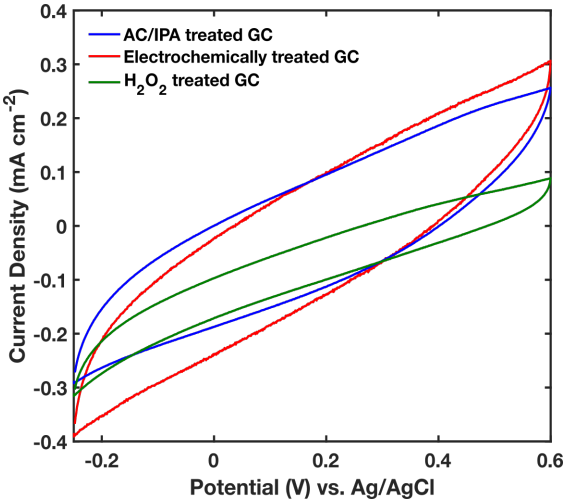


Figure S7: Current density versus potential data for AC/IPA treated, electrochemically treated and $H_2O_2$ treated GC electrodes in 0.5 M $H_2SO_4$(aq) solution.

The observed residual surface roughness resulting from polishing complicates quantitative analysis of electron transfer rates due to the increase in electrochemically accessible surface area per unit geometric area. We made extensive efforts to determine the origin of this residual roughness, and ultimately determined it to be due to the use of low-quality silicon carbide media to grind the GC electrodes flat prior to the initiation of alumina polishing steps. However, prior

work on GC has clearly shown that it is not possible to entirely remove surface roughness through abrasive polishing alone.[8] Moreover, even GC electrodes with completely smooth surfaces would exhibit considerable site heterogeneity arising from the high density of crystallographic defects, which makes the determination of the "intrinsic" kinetics of these electrodes difficult. In fact, we argue that consistent, moderate surface roughness may be advantageous for the study of RFB kinetics, in that it is likely to expose more structurally diverse active sites, as would be expected to exist in high surface-area carbon materials that are used in functional devices. In this context, kinetic limitations can be considerably ameliorated by using porous carbon electrodes with very high roughness factors, but we still see a significant advantage in determining the types of surface functionality that are the most stable and catalytically active, even if the final benefit is mainly in increasing the wettability of the electrode.

## Exchange current density normalized to carbonyl content

Figure S8 presents bar chart of exchange current density normalized to the fractional coverage of carbonyl obtained from XPS. As seen from the figure, the carbonyl normalized exchange current density is the highest for electrochemically treated GC followed by AC/IPA treated GC and $H_2O_2$ treated GC.

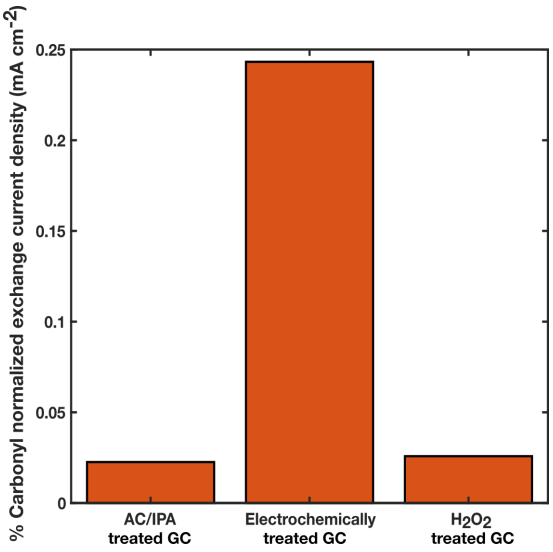


Figure S8: Bar chart of exchange current density normalized to % carbonyl content for all carbon treatments

## Additional discussion of XPS surface oxidation measurements

XPS is a surface sensitive technique that nevertheless probes a volume extending some distance into the sample. Often the XPS probe depth is assumed to be a few nm so that the data can be treated as qualitatively indicative of the surface composition of a sample. However, because we observed only small changes in apparent oxidation after treating GC surfaces, we were interested in a more quantitative estimate of the degree of surface oxidation that would result in a particular increase in XPS signal corresponding to oxidized carbon. Thus, we estimated an XPS probe depth not in terms of distance, but in terms of the total number of carbon atoms in GC that are sampled by an XPS measurement. To do so, we used Equation 4, which describes the probability $P(d)$ of a photoelectron escaping from a depth $d$ within a solid:

$$P(d) = exp\left(\frac{-d}{\lambda \cos\theta}\right) \tag{4}$$

where $\lambda$ is the material and energy-dependent inelastic mean free path of the electron (31.06 Å at electron energy of 1196 eV in this case[9]) and $\theta$ is the angle between the detector and normal to the

sample (40° in this case). Thus the term $\lambda cos(\theta)$ is an effective mean free path where $\lambda_{\text{eff}} = 23.8$ Å that takes into account the acceptance angle of the detector in the XPS measurement.

Next we approximated the GC near the surface region as a bulk solid comprised of essentially parallel layers separated by an average C−C distance of 2.2 Å, which is the arithmetic mean of three covalent bond lengths (1.42 Å) and two Van der Waals bond lengths (3.41 Å) in graphite (Figure S9). This allowed us to approximate the total number of carbon atoms sampled by the XPS measurement in the z direction (normal to the surface) as the number of C−C distances required to reach a depth of 3 effective mean free paths ($3 \cdot 23.8/2.2 \approx 33$) weighted by the probability of electron escape at the depth of each individual layer, as in Equation 5.

$$C = \sum_{n=0}^{33} P(n \cdot 2.2) \tag{5}$$

where $n$ refers simply to a layer index beginning at the surface (n=0) and ending at a depth equal to $3\lambda_{\text{eff}}$ (n=33). In this way, we found $C$ to be 10.7, which implies that a GC sample with zero bulk oxygen content and monolayer surface coverage of oxygen would correspond to an apparent fraction of oxidized carbon on the order of 9 % by XPS.

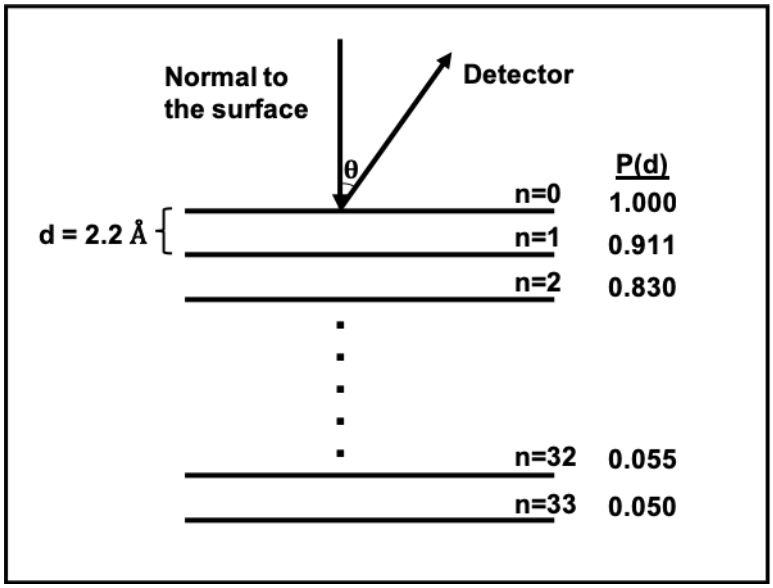


Figure S9: Schematic representation of carbon layers from n=0 to n=33 ($\sim 3\lambda_{\text{eff}}$), each separated by an average distance of 2.2 Å, along with the diminishing probabilities of electron escape in each layer.

# References

(1) Štulíková, M.; Vydra, F. Voltammetry with Disk Electrodes and its Analytical Application: IV. The Voltammetry of Iron(III) at the Glassy Carbon Rotating Disk Electrode in Acid Media. *J. Electroanal. Chem. Interf. Electrochem.* **1972**, *38*, 349–357.

(2) Galus, Z.; Adams, R. N. The Investigation of the Kinetics of Moderately Rapid Electrode Reactions using Rotating Disk Electrodes. *J. Phys. Chem* **1963**, *67*, 866–871.

(3) McDermott, C. A.; Kneten, K. R.; McCreery, R. L. Electron Transfer Kinetics of Aquated Fe (+3/+2), Eu(+3/+2), and V(+3/+2) at Carbon Electrodes: Inner Sphere Catalysis by Surface Oxides. *J. Electrochem. Soc.* **1993**, *140*, 2593–2599.

(4) Hawthorne, K. L.; Wainright, J. S.; Savinell, R. F. Studies of Iron-Ligand Complexes for an All-Iron Flow Battery Application. *J. Electrochem. Soc.* **2014**, *161*, A1662–A1671.

(5) Ateya, B. G.; Austin, L. G. The Kinetics of Fe(2+)/ FeCl(2+)/ HCI (aq) on Pyrolytic Graphite Electrodes. *J. Electrochem. Soc.* **1973**, *120*, 1216–1219.

(6) Nicholson, R. S. Theory and Application of Cyclic Voltammetry for Measurement of Electrode Reaction Kinetics. *Anal. Chem* **1965**, *37*, 1351–1355.

(7) Ranganathan, S.; Kuo, T. C.; McCreery, R. L. Facile Preparation of Active Glassy Carbon Electrodes with Activated Carbon and Organic Solvents. *Anal. Chem* **1999**, *71*, 3574–3580.

(8) McDermott, M. T.; McDermott, C. A.; McCreery, R. L. Scanning Tunneling Microscopy of Carbon Surfaces: Relationships between Electrode Kinetics,Capacitance, and Morphology for Glassy Carbon Electrodes. *Anal. Chem.* **1993**, *65*, 937–944.

(9) Shinotsuka, H.; Tanuma, S.; Powell, C. J.; Penn, D. R. Calculations of Electron Inelastic Mean Free Paths. X. Data for 41 Elemental Solids over the 50 eV to 200 keV Range with the Relativistic Full Penn Algorithm. *Surf. Interface Anal.* **2015**, *47*, 871–888.